

# Catalytic Microstrider at the Air–Liquid Interface

By Alexander A. Solovev, Yongfeng Mei,\* and Oliver G. Schmidt

Inspired by water striders in nature<sup>[1,2]</sup> there is great interest to build artificial water-walking devices.<sup>[3–5]</sup> Meanwhile, motion in fluids at the micro- and nanoscale have generated ever new ideas and concepts to overcome the high viscosity problem at low Reynolds numbers.<sup>[6–9]</sup> Up to date there have been a few demonstrations of micro-/nanoscale water-walking devices, and self-assembly of catalytic micro-/nanoscale motors can be driven by capillary forces.<sup>[10]</sup> Here, we show that a rolled-up catalytic micro-/nanotube can act as a strider at the air–liquid interface of hydrogen peroxide (H<sub>2</sub>O<sub>2</sub>) solution. Such micro-/nanotubes buoyed and self-propelled by oxygen bubbles move at the fuel surface by bubble recoiling, and easily land on micro-objects by the meniscus-climbing effect, which is one of the main features found in the behavior of water striders.<sup>[11]</sup> The balance between capillary and drag forces determines assembly and disassembly of the microtubes, which thus exemplifies a dynamic self-assembly behavior of micromachines on the micro- and nanoscale.

We use rolled-up nanotechnology<sup>[12,13]</sup> to construct Ti/Cr/Pt microtubes with diameters of 5–10 μm and length of ~50 μm, where the Pt metal acting as a catalyst is well confined inside the tubes to decompose H<sub>2</sub>O<sub>2</sub> into water and oxygen.<sup>[14]</sup> The confined tubular geometry collects oxygen as bubbles, which are ejected from one of the tube ends and thus recoils (propels) the microtube. In order to demonstrate the strider behavior of our microtubes at the air–liquid interface, we create a thin aqueous film by adding a drop of 30% H<sub>2</sub>O<sub>2</sub> aqueous solution on propylene carbonate (PC), which is intermixed with catalytic microtubes. After fuel addition, H<sub>2</sub>O<sub>2</sub> diffuses into PC<sup>[15]</sup> and activates/lifts the catalytic microtubes to the solution surface due to the buoyancy force of oxygen bubbles in liquid. These self-propelled catalytic micromachines move at the aqueous surface for minutes until the fuel (here H<sub>2</sub>O<sub>2</sub>) is consumed. We estimate the buoyancy force and the weight of a catalytic microtube. If half of the tube with a 5 μm diameter and a 50 μm length is full of O<sub>2</sub> gas, the induced buoyancy force is around 5 pN in propylene carbonate (PC) or water. The buoyancy force in PC is ~1.2 times larger than that in water due to the density. However, the weight of a tube with the same 5 μm diameter is around 2.5 pN for the Ti/Cr/Pt (5/5/2 nm in thickness) composition. Since the buoyancy force depends on the gas generated in the tube, we can derive the filling volume of gas in the tube. Because PC with a slightly higher density (1.205 g/ml) can lift the striders but water can not, it means that the buoyancy force

in water is smaller than the weight of the tube, but that in PC is bigger. We thus can deduce that the buoyancy force in water and PC should be very close to the weight of 2.5 pN, which is roughly the buoyancy force generated in one quarter of the tube. As a result, the filling volume of gas in the tube is around one quarter of the body volume of our catalytic striders, which thus is enough to take the striders to the air–liquid interface.

We found that catalytic microtubes firmly attached to bubbles can attract each other at an aqueous fuel surface and self-assemble into patterns due to the meniscus-climbing effect as sketched in **Figure 1a**. Bubbles pull attached microtubes together and form self-assembled structures of microtubes (a colony in S-Figure 1a and an array in Figure 1b). The microtubes are well aligned in certain directions and pile up in abundance (Figure 1b). Once the existed bubbles break, the micromachines separated but sometimes return depending on the balance between the attractive capillary due to new generated bubbles and repulsive driving forces. Such a balanced system offers an intriguing way to study dynamic self-assembly. By tuning the surface tension of the fuel, the attaching and detaching times of bubbles to and from microtubes can be adjusted for controllable dynamic self-assembly. For example, we can completely mix PC with H<sub>2</sub>O<sub>2</sub> aqueous solution (up to 1:5 v/v) as a fuel since PC is soluble to large extent in water (~20 wt%).<sup>[15]</sup> This mixture still easily powers the micromachines, but the bubbles break immediately after ejection from the tube ends. Hence, the catalytic microtubes run independently at the surface without attraction (S-Figure 1b). It is noticed that with a pure aqueous H<sub>2</sub>O<sub>2</sub> solution with surfactants, the catalytic microtube machines run independently as well but inside the fluid not at the surface.<sup>[14]</sup> We deduce that bubbles in PC generate a stronger buoyancy force compared to that in water, and thus drives the catalytic microtubes to the surface, since the density of PC (1.205 g/ml) is higher than that of water.

The attracting capillary force induced by the meniscus-climbing effect was easily studied by inserting a glass capillary into the surface to anchor our micromachines. As displayed in Figure 1c, a glass capillary is inserted into a fuel surface. Several catalytic micromachines moving around previously rush spontaneously towards the capillary at the liquid surface. Individual images for three microtubes are shown in Figure 1d–f, which correspond to the tubes i–iii shown in Figure 1c, respectively. As schematically shown in the inset of Figure 1c, a generated bubble with a connected tube is pulled towards a micro-object (here glass capillary) by the capillary force ( $F_c$ ), while the buoyancy force ( $F_b$ ) from the bubbles lifts the tube to the fluid surface. Such a landing or climbing behavior of our artificial micromachines is similar to that of water-walking insects like *Mesovelia*, *Hydrometra* and the beetle larva.<sup>[11]</sup> In addition, the blocking effect of catalytic engines by bubbles described in Ref.<sup>[14]</sup> may also support the self-assembly of our striders by ceasing the catalytic reaction. In this case closely packed tubes

[\*] A. A. Solovev, Dr. Y. F. Mei, Prof. O. G. Schmidt  
Institute for Integrative Nanosciences  
IFW Dresden  
Helmholtzstr. 20, Dresden, 01069 (Germany)  
E-mail: y.mei@ifw-dresden.de

DOI: 10.1002/adma.201001468

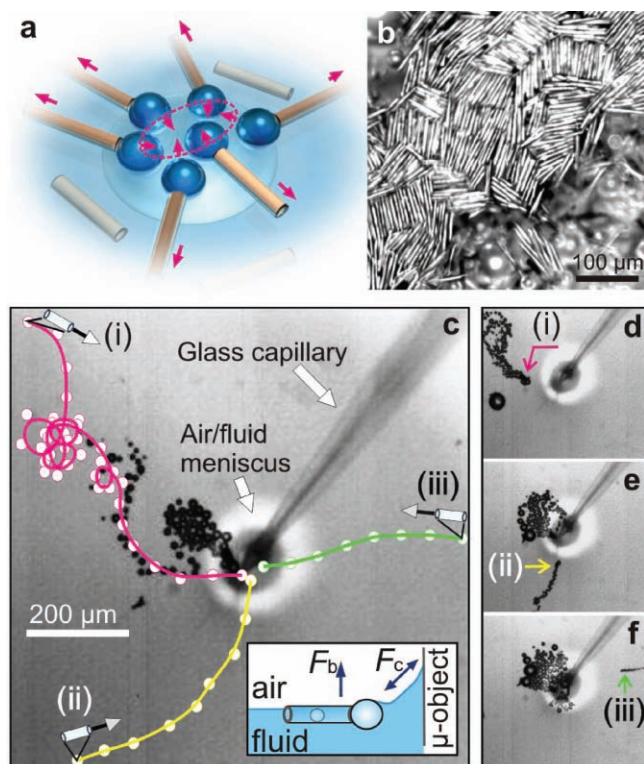


**Figure 1.** a) Schematic illustration of bubble-attached catalytic microtubes attracted to each other. The individual arrows represent the repulsion forces due to the bubble recoiling mechanism, while the arrows within the dashed circle denote the meniscus-climbing effect (attraction) initiated by capillary forces. b) Optical image of a self-assembled microtube array, where 100  $\mu\text{L}$  30%  $\text{H}_2\text{O}_2$  fuel was added into 200  $\mu\text{L}$  PC. c) The Meniscus-climbing microtubes (i-iii) rushing towards a glass capillary. The lines and solid circles show the corresponding trajectories for each tube. d-f) selected video frames for the individual microtubes in (c). The arrows highlight the moving microtubes.

can decrease the catalytic reaction rate, leading to closely packed assembly shown in Figure 1b.

The capillary force among water-walking insects also enables them to attract each other and to self-assemble into a colony,<sup>[16]</sup> which is similar to our catalytic strider behavior at the air-liquid interface described above. Interestingly, the self-assembly of our micromachines reveal a dynamic characteristic, which mainly depends on the fuel concentrations. As shown in the top image of Figure 2a, several catalytic micromachines have gathered into a colony after adding one drop of  $\text{H}_2\text{O}_2$  solution. The resultant trajectories of several microtubes within one second are shown in the bottom image of Figure 2a. However, after several seconds these powered catalytic microtubes disassemble due to their reduced power since the fuel is being consumed. As revealed in Figure 2b, the micromachines are dispersed  $\sim 10$  seconds after Figure 2a is recorded. The gradual separation of all microtubes is revealed by their trajectories (see bottom image of Figure 2b). The tubes do not aggregate again until fuel is refilled. We note that as long as sufficient fuel is provided, we observe a cyclic behavior of assembly and disassembly of the catalytic micromachines.

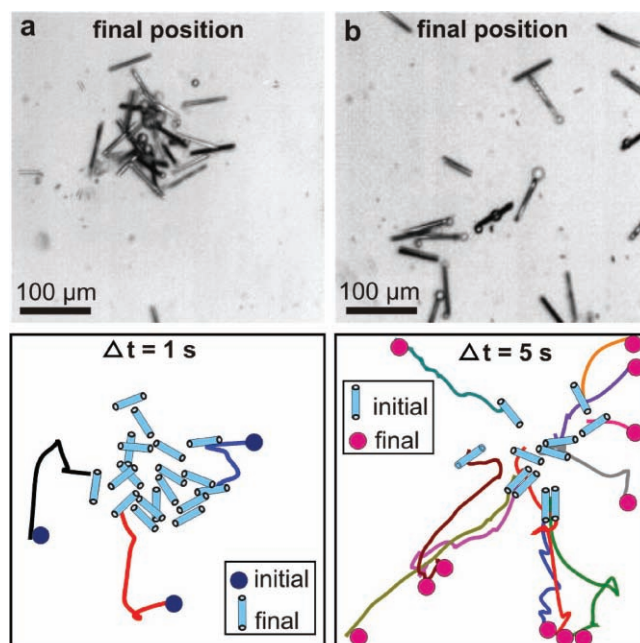


**Figure 2.** a, (top) Optical image of powered catalytic microtubes assembling into a colony after adding a drop of hydrogen peroxide solution (20  $\mu\text{L}$  30%  $\text{H}_2\text{O}_2$ ) into 100  $\mu\text{L}$  PC. (bottom) Recorded trajectories leading to the top image within one second. b, (top) Optical image of powered catalytic microtubes disassembled after several seconds. (bottom) Recorded trajectories leading to the top image within five seconds. Notice that the final position in a is not the initial position in (b). There are several seconds between (a) and (b) without recording.

We also carried out a statistical analysis of the disassembly behavior described above. The original video frames are taken from S-Figure 1a and S-Video 4 for examination. We choose one-second videos when the micromachines change from the “self-assembly” state to the disperse state. The average bubble radius as a function of time is shown in Figure 3a. The bubble radius reduces with time, while the micromachines separate more and more (sketched in the insets). Basically, two major conditions influence the bubble size. One is the fuel concentration, where higher concentrations lead to smaller bubbles.<sup>[14]</sup> The other is the surface tension of the fluid. We tested the micromachine velocity in a constant  $\text{H}_2\text{O}_2$  concentration but with various ratios of water in PC (fully mixed), which slightly changes the surface tension.<sup>[17]</sup> As presented in Figure 3b, the bubble radius becomes smaller when decreasing the ratio of water in PC, while the micromachine velocity increases even with a constant fuel concentration. Hence, we can explain why powered catalytic microtubes disassemble with time in the case of adding a drop of  $\text{H}_2\text{O}_2$ . When the tubes become disperse, the bubble radius reduces (Figure 3a) and thus the attracting force decreases.<sup>[17]</sup> However, the velocity still could rise due to the evaporation of water because of Figure 3b, which means the drag force responsible for dispersion is enhanced. Therefore, the micromachines disassemble with time.

The velocity and bubble size play a critical role for the assembly of our microtube machines. As shown in Figure 4a, three typical microtube machines are selected for analysis with

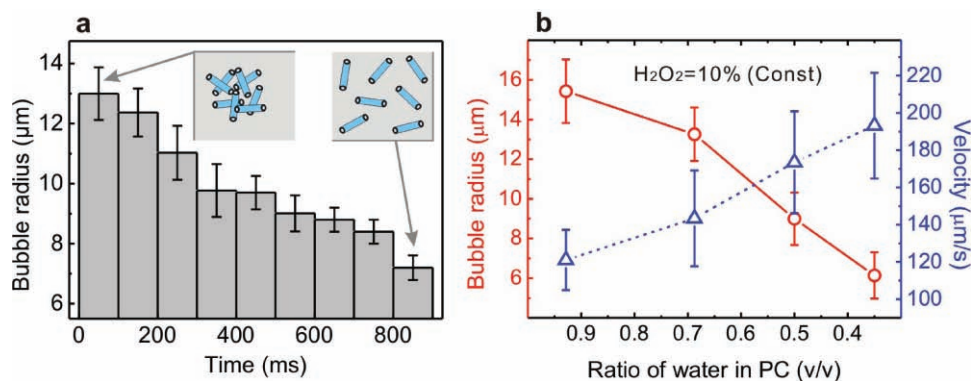


**Figure 3.** a) Bubble radius as a function of time. The data is taken from S-Figure 1a and S-Video 4. The insets sketch the assembly and disassembly behaviors of the micromachines for the indicated time. b) Bubble radius and velocity of catalytic microtubes as a function of ratio of water in PC (v/v) at a constant concentration of  $\text{H}_2\text{O}_2$  (10%).

bubble sizes of around 5, 12, 21  $\mu\text{m}$  (microtube #1, #2, and #3, respectively). Connected circles in Figure 4a mark their trajectories. #1 moves away from the huge central bubble; #2 moves in a dynamic equilibrium; while #3 runs towards the big bubble. This observation confirms our explanation of Figure 3, where small bubbles tend to lead to a disassembly behavior. Further analysis in Figure 4b and c discloses the kinematic characteristics of the three tubes including traveling distance and velocity with time. We treat the distance and velocity along a trajectory away from (towards) the huge central bubble as a positive (negative) value. The micromachine #1 generating small bubbles (below 5  $\mu\text{m}$ ) runs away from the huge central bubble, which is indicated by a positive and increasing travel distance (b) as well

as a positive velocity (c). The micromachine #3 with big bubbles ( $\sim 21 \mu\text{m}$ ) is rushing into the huge central bubble, which is reflected by a negative and increasing travel distance as well as a negative velocity. The micromachine #2 with mediate bubbles ( $\sim 12 \mu\text{m}$ ) finds itself in a dynamic equilibrium state, and walks forth [labeled as (i)] and back (ii) for several times. This effect is generated by the balance between the attractive capillary and repulsive motive force from bubbles.

Generally, water striders in nature can attract neighbours over a distance comparable to the capillary length (approximately their body length).<sup>[16]</sup> Fialkowski et al. have described a two-spheres system (with center-to-center distance  $L$ ) with a capillary force  $F_c \propto \gamma R^2/L$ , where  $\gamma$  is the surface tension of the applied liquid

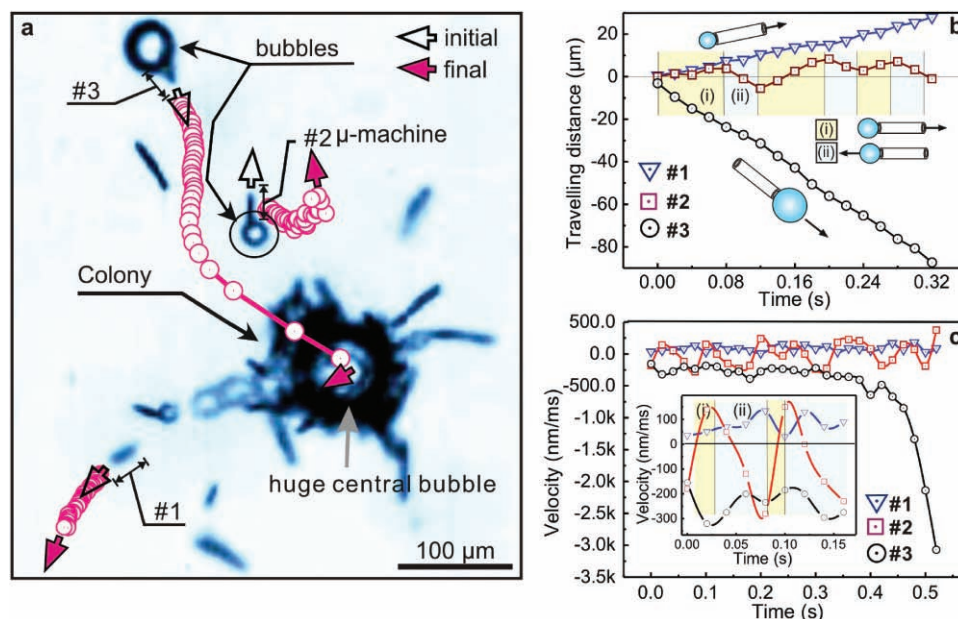


**Figure 4.** Analysis of individual catalytic striders at the air–liquid interface interacting with a big bubble. a) Optical image showing dynamics of three micromachines (#1, #2, and #3), where #1 is leaving away from the bubble; #2 is in a dynamic equilibrium; while #3 is running to the bubble. Kinematics: travelling distance (b) and velocity (c) with time of three individual micromachines.

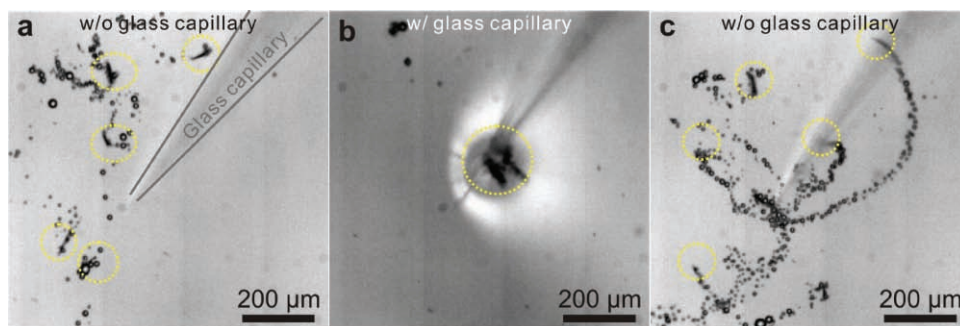


**Figure 5.** Reproducible demonstration of the Meniscus-climbing microtubes (highlighted by yellow circles) rushing towards a glass capillary. **a**) The microtube striders undergo random motions at the air–liquid interface without the glass capillary inserted. **b**) The microstriders attach to the glass capillary immersed into the liquid; the dark and highlighted area (yellow circle) are the tubes. **c**) Once the glass capillary is removed, the catalytic striders (highlighted by yellow circles) move away randomly.

and  $R$  is the radii of the spheres.<sup>[18]</sup> So the attractive capillary force increases with the radii of the spheres. If we apply this principle to our system, big bubbles (with big radii) can supply a stronger capillary force for attraction and small ones produce a relatively weak force. The strider driving force is due to continuously generated microbubbles with a certain frequency and size.<sup>[14]</sup> However an attraction originates from the generated bubbles connected to a strider. The connection time between the bubbles and striders is relatively short (maximum estimated tens of milliseconds) for bubbles in mixture of hydrogen peroxide and propylene carbonate. Thus, as long as the generated bubbles are connected to striders they attract them, but when bubbles break away, the attraction ceases and striders move apart. Hence, if the driving force is higher than the weak attraction force between small bubbles, the microengines move away from the positive menisci curvature created by a glass capillary. More generally, when distances between bubbles or between bubbles and glass capillaries are comparable to the size of bubbles or glass capillaries (take the bigger one), the attraction force leads to capture of the catalytic microengines. Based on the equation  $F_c \propto \gamma R^2/L$ , one could deduce that the capillary force (i.e. attraction force) reduces with the decrease of the bubble size.<sup>[18]</sup> The striders in the same system have similar driving force, but smaller bubbles lead to a weaker capillary attraction force compared to the driving force. Hence, the striders with smaller bubbles leave the glass capillary, which is exactly the behavior of the #1 tube in Figure 4. Moreover, we introduced a micro-object to replace the huge central bubble as shown in S-Figure 2. The catalytic micromachines can still move around and climb the defined object, which thus strengthens our above interpretation.

A reproducible demonstration of the meniscus-climbing effect has also been revealed. At first the glass capillary is positioned above the liquid surface, and random motion of the catalytic microstriders (highlighted by yellow circles) is observed in Figure 5a. Once the glass capillary is immersed into the liquid fuel, the striders run towards the capillary and attach to it (Figure 5b). The black area in the center (close to the capillary tip, highlighted by yellow circles) is populated by the attached tubes. When the capillary tip is removed from the liquid, all striders (highlighted by yellow circles) still stay at the air–liquid interface but move away randomly. The bubble tails reveal their trajectories. This demonstration

has been reproduced 6 times as shown in the Supporting Information – Video 8, and proves our concept of catalytic microstriders at the air–liquid interface.

In summary, we have demonstrated self-powered microstriders at the air–liquid interface made of rolled-up catalytic microtubes. The meniscus-climbing effect – ubiquitous for water walking insects – is well-documented for this type of artificial micro strider by several experiments. The balance between capillary and drag forces determines assembly and disassembly of the microtubes, which is attractive to study dynamic self-assembly on the micro- and nanoscale.<sup>[10,18]</sup> Our work is helpful to understand future bio-inspired robotics, in particular if interactions among an ensemble of micro- and nanomachines in fluids needs to be considered.

### Experimental Section

Catalytic Ti/Cr/Pt microtubes were fabricated by e-beam deposition of metallic layers onto lithographically-patterned photoresist layers. Square photoresist patterns with a width of 50 nm were prepared on 1.5 inch silicon wafers. Photoresist AR-P 3510 was spin coated onto silicon wafers at 3500 rpm for 35 seconds, followed by a soft bake using a hotplate at 90 °C for 1 minute and exposure to UV light with a Karl Suss MA56 Mask Aligner (410–605 nm). Patterns were developed in a v/v 1:1 AR300–35:H<sub>2</sub>O solution. By dissolving the photoresist layer in acetone solution, pre-stressed multilayers automatically rolled up into microtubes. The supercritical point dryer was adopted in the fabrication of rolled-up microtubes to avoid the tube collapsing due to the surface tension of the aqueous etchants. Under an optical microscope still images were captured by a Zeiss Axiocam MRc camera and live videos were recorded by using a Photonic Science Dalsa high-speed camera at 50 frames per second.

### Supporting Information

Supporting Information is available from the Wiley Online Library or from the author.

### Acknowledgements

We are grateful for fruitful discussion by Hengxing Ji and Samuel Sanchez, and experimental help by Ronny Engelhard and Cornelia Krien.

This work was financially supported by the Grant from the Volkswagen Foundation (I/84 072). YFM also thanks to the support from the Visiting Scholar Foundation of Key Lab. of Opto-electronic Technology and Systems In Chongqing University.

Received: April 21, 2010

Published online: August 20, 2010

- 
- [1] D. L. Hu, J. W. M. Bush *Nature* **2003**, 424, 663.
- [2] X. Gao, L. Jiang, *Nature* **2004**, 432, 36.
- [3] S. Floyd, M. Sitti, *IEEE Tran. Robot.* **2008**, 24, 698.
- [4] L. Jiang, X. Yao, H. Li, Y. Fu, L. Chen, Q. Meng, W. Hu, L. Jiang, *Adv. Mater.* **2010**, 22, 376.
- [5] D. L. Hu, M. Prakash, B. Chan, J. W. M. Bush, *Exp. Fluids* **2007**, 43, 769.
- [6] E. M. Purcell, *Am. J. Phys.* **1977**, 45, 3.
- [7] G. A. Ozin, I. Manners, S. Fournier-Bidoz, A. Arsenault, *Adv. Mater.* **2005**, 17, 3011.
- [8] W. F. Paxton, S. Sundararajan, T. E. Mallouk, A. Sen, *Angew. Chem. Int. Ed.* **2006**, 45, 5420.
- [9] K. Manesh, J. Wang, *Small* **2010**, 6, 338.
- [10] a) T. R. Kline, J. Iwata, P. E. Lammert, T. E. Mallouk, A. Sen, D. Velegol, *J. Phys. Chem. B* **2006**, 110, 24513; b) P. Dhar, Th. M. Fischer, Y. Wang, T. Mallouk, A. Sen, *Nano Lett.* **2006**, 6, 66; c) Y. Wang, S-t Fei, Y.-M. Byun, P. E. Lammert, V. H. Crespi, A. Sen, T. E. Mallouk, *J. Am. Chem. Soc.* **2009**, 131, 9926.
- [11] D. L. Hu, J. W. M. Bush, *Nature* **2005**, 437, 733.
- [12] O. G. Schmidt, K. Eberl, *Nature* **2001**, 410, 168.
- [13] Y. F. Mei, G. S. Huang, A. A. Solovev, E. Bermúdez Ureña, I. Moench, F. Ding, T. Reindl, R. K. Y. Fu, P. K. Chu, O. G. Schmidt, *Adv. Mater.* **2008**, 20, 4085.
- [14] A. A. Solovev, Y. F. Mei, E. Bermúdez Ureña, G. S. Huang, O. G. Schmidt, *Small* **2009**, 5, 1688.
- [15] G. Palazzo, D. Fiorentino, G. Colafemmina, A. Ceglie, E. Carretti, L. Dei, P. Baglioni, *Langmuir* **2005**, 21, 6717.
- [16] J. W. M. Bush, D. L. Hu, M. Prakash, *Adv. Insect Physiol.* **2008**, 34, 118.
- [17] The surface tension value for PC at 20°C is 41.93 dyn/cm (<http://macro.lsu.edu/HowTo/solvents/Propylene%20Carbonate.htm>), while it is 72.8 dynes/cm for Water at 20°C (<http://hyperphysics.phy-astr.gsu.edu/Hbase/surten.html>).
- [18] M. Fialkowski, K. J. M. Bishop, R. Klajn, S. K. Smoukov, C. J. Campbell, B. Grzybowski, *J. Phys. Chem. B* **2006**, 110, 2482.
-